

# Maximizing CNN Accelerator Efficiency Through Resource Partitioning

Yongming Shen  
Stony Brook University  
yoshen@cs.stonybrook.edu

Michael Ferdman  
Stony Brook University  
mferdman@cs.stonybrook.edu

Peter Milder  
Stony Brook University  
peter.milder@stonybrook.edu

**Abstract**—Convolutional neural networks (CNNs) are revolutionizing a variety of machine learning tasks, but they present significant computational challenges. Recently, FPGA-based accelerators have been proposed to improve the speed and efficiency of CNNs. Current approaches construct a single processor that computes the CNN layers one at a time; this single processor is optimized to maximize the overall throughput at which the collection of layers are computed. However, this approach leads to inefficient designs because the same processor structure is used to compute CNN layers of radically varying dimensions.

We present a new CNN accelerator paradigm and an accompanying automated design methodology that partitions the available FPGA resources into multiple processors, each of which is tailored for a different subset of the CNN convolutional layers. Using the same FPGA resources as a single large processor, multiple smaller specialized processors result in increased computational efficiency and lead to a higher overall throughput. Our design methodology achieves 1.51x higher throughput than the state of the art approach on evaluating the popular AlexNet CNN on a Xilinx Virtex-7 FPGA. Our projections indicate that the benefit of our approach increases with the amount of available FPGA resources, already growing to over 3x over the state of the art within the next generation of FPGAs.

## I. INTRODUCTION

The rapid adoption of convolutional neural networks (CNNs) has transformed machine learning. CNNs have been embraced across a wide array of fields, such as recommendation systems [1], natural language processing [2], and computer vision [3]. In particular, image object recognition has become the de facto benchmark for CNNs, with new networks shattering all prior records in object detection and classification every year.

However, improvements in CNN accuracy are accompanied by a rapid increase in computational cost. CNNs have already grown to the point where multi-core CPUs are no longer a viable computing platform. At the same time, while GPUs offer adequate performance, GPU power consumption brings its own set of challenges, particularly at data-center scale. As a result, FPGAs have seen a surge in interest for CNN acceleration due to their programmable, massively parallel, and power-efficient computing substrate.

CNNs comprise multiple computation *layers*, whose inputs are arrays of different dimensions, given by the CNN specification. The state of the art for using FPGAs for CNNs is to implement an accelerator that we call a *convolutional layer processor* (CLP), which iteratively processes the layers, one at a time. A CLP design depends on parameters that control the

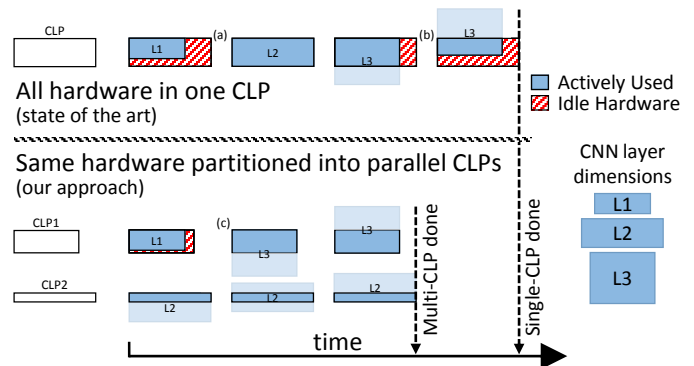


Fig. 1. Operation of convolutional layer processors (CLPs) on a three-layer CNN. Both Single-CLP (state-of-the-art) and Multi-CLP (our approach) use the same total hardware resources. Multi-CLP partitioned hardware closely matches the CNN layers, minimizing idle hardware and improving performance.

dimensions of its computational grid; its speed depends on the compatibility of these dimensions with the CNN layers it computes. CLP parameters are jointly optimized for the ensemble of the layers in a way that maximizes the collective throughput of the accelerator.

We observe that jointly optimizing a single CLP for all CNN layers leads to dynamic underutilization of FPGA resources. Although the CLP is optimized for maximum throughput, the fixed dimensions of the CLP computational grid are sub-optimal for some, or even all, of the individual layers. Figure 1 (top) illustrates this problem. The Single-CLP hardware (white box) iteratively processes the three layers (blue boxes). The dimensions of the hardware and the layers are represented by the size and shape of the boxes. L1 is smaller than the CLP dimensions, leaving some hardware unused when computing this layer (Figure 1(a)). L2 size exactly matches the CLP, but L3 dimensions exceed the CLP size. Therefore, the CLP computational grid must be used iteratively to compute different parts of L3 (first, its top portion, then, its bottom portion), again underutilizing the available hardware (Figure 1(b)). On the popular AlexNet CNN [3], an “optimal” Single-CLP derived from the state-of-the-art methodology [4] has dynamic utilization of less than 66%. This means that, on average, more than one third of the computational resources dedicated to the CLP are unused.

To overcome this problem, we propose a new CNN accel-

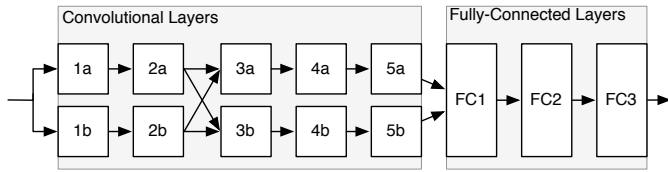


Fig. 2. AlexNet CNN structure [3].

erator design that partitions the available hardware resources among multiple CLPs, which operate on multiple images concurrently. We illustrate such a Multi-CLP system in Figure 1 (bottom), where the hardware resources are now partitioned into two smaller CLPs that operate in parallel on different images. Note that the two CLPs are specialized and have different dimensions; this allows CLP1 to fit well with L1 and L3, while CLP2 dimensions are compatible with L2. The key is to note that these sizes allow the layers to be processed with very little idle hardware, allowing the Multi-CLP to do the same amount of work in less time (Figure 1(c)).

We develop an optimization algorithm that, given CNN layer dimensions and resource budget, computes a partitioning of the FPGA resources into multiple CLPs for an efficient high-performance design. Our algorithm runs in minutes on a modern system and produces a set of CLP dimensions. We then use these dimensions to parameterize an HLS-based CLP design, combining the resulting CLPs to form a complete CNN implementation.

Our results on AlexNet demonstrate that partitioning FPGA resources into multiple CLPs achieves 99% dynamic DSP utilization, improving performance by 51% over the state-of-the-art methodology when targeting a Xilinx Virtex-7 FPGA. More importantly, we project the future performance of our methodology and find that the speedup increases rapidly with the available FPGA resources, already growing over 3x when targeting the resources that will be available in the next generation of FPGAs.

The rest of the paper is organized as follows. In Section II, we provide background on CNNs. Section III describes the state-of-the-art FPGA implementation and analyzes the inefficiency of Single-CLP accelerators. Section IV presents our Multi-CLP optimization methodology. Section V describes our design and implementation and Section VI details experimental results. Section VII discusses related work. We conclude in Section VIII.

## II. CNN BACKGROUND

In typical object recognition examples (e.g., [3], [5]), a CNN passes images through a number of convolutional layers, which convolve the input (an array of two-dimensional matrices called feature maps) with an array of two-dimensional filters, whose values (called weights) were previously learned using an algorithm such as back-propagation. Non-linear layers, which typically perform computations such as subsampling or activation functions, interleave convolutional layers. In the end, the network includes one or more fully-connected layers,

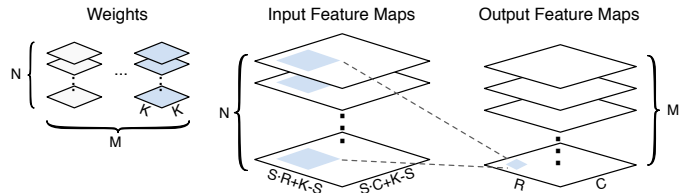


Fig. 3. Illustration of a convolutional layer.

```

I[N][[R-1]*S+K][[C-1]*S+K] //input feature maps
O[M][R][C] //output feature maps
W[M][N][K][K] //weights
for (m = 0; m < M; m++)
  for (n = 0; n < N; n++)
    for (r = 0; r < R; r++)
      for (c = 0; c < C; c++)
        for (i = 0; i < K; i++)
          for (j = 0; j < K; j++)
            O[m][r][c] += W[m][n][i][j] * I[n][S*r+i][S*c+j]

```

Listing 1. Pseudo code of a convolutional layer.

each of which performs a number of dot-products across its entire input. Figure 2 provides an example of AlexNet [3], which contains 5 stages of paired convolutional layers (e.g. 1a and 1b), followed by three stages of fully-connected layers (FC1–FC3). In this figure, the small non-linear layers are omitted. As in prior work [4], we focus on the convolutional layers of the network and assume all data are single-precision floating point.

Figure 3 illustrates a convolutional layer and Listing 1 presents the pseudo-code to compute it. Each layer takes as input a set of  $N$  input feature maps and convolves them with the filters. There are  $M$  sets of filters; by convolving one set of  $N$  filters ( $N \times K \times K$  weights) with the input feature maps, one of the  $M$  output feature maps is obtained.<sup>1</sup> For example, the blue point in the lowest output feature map in Figure 3 is computed by taking the dot-product of the blue weights with the portion of the input feature maps shaded blue. By sliding this blue shaded region around the input feature maps, we can fill in all of the points on this output feature map. By repeating this process with each of the  $M$  sets of filters, we compute each of the  $M$  output feature maps. Each output feature map also has a bias value associated with it that is added to every pixel. We omit bias in the figure for simplicity.

## III. RESOURCE UTILIZATION PROBLEM

A common approach for building a CNN accelerator is to construct what we call a *convolutional layer processor* (CLP), which computes the nested loop in Listing 1. Since a CNN has multiple convolutional layers, the same CLP is used to process all layers, one by one. Because different convolutional layers have different dimensions ( $M, N, R, C, K, S$ ), such a “one size fits all” approach creates a resource utilization problem,

<sup>1</sup>The convolution can use a stride  $S$ , where each step shifts the region by  $S$ .

```

I[N][[(R-1)*S+K][(C-1)*S+K]] //input feature maps
O[M][R][C] //output feature maps
W[M][N][K][K] //weights
I_buf[T_n][[(T_r-1)*S+K][(T_c-1)*S+K]] //input buffer
O_buf[T_m][T_r][T_c] //output buffer
W_buf[T_m][T_n][K][K] //weight buffer
for (r=0; r<R; r+=T_r)
  for (c=0; c<C; c+=T_c)
    for (m=0; m<M; m+=T_m) {
      for (n=0; n<N; n+=T_n) {
        I_buf = I[n:n+T_n][r*S:(r+T_r-1)*S+K][c*S:(c+T_c-1)*S+K]
        W_buf = W[m:m+T_m][n:n+T_n]
        for (i=0; i<K; i++)
          for (j=0; j<K; j++)
            for (tr=0; tr+r<min(R, r+T_r); tr++)
              for (tc=0; tc+c<min(C, c+T_c); tc++)
                for (tm=0; tm<T_m; tm++) #UNROLL
                  for (tn=0; tn<T_n; tn++) #UNROLL
                    O_buf[tm][tr][tc] +=
                      W_buf[tm][tn][i][j]*I_buf[tn][S*tr+i][S*tc+j]
      }
      O[m:m+T_m][r:r+T_r][c:c+T_c] = O_buf
    }

```

Listing 2. Pseudo code for tiling in a convolutional layer processor [4].

as illustrated in Figure 1. In this section, we analyze how this problem affects a state of the art FPGA CNN accelerator.

### A. State of the Art Design

The design in [4] is the state of the art for FPGA acceleration of CNN convolutional layers. It employs loop transformations, such as loop reordering, tiling, and unrolling to reorder computations and memory accesses, increasing throughput and reducing data transfer. The transformed loop is used as a template for constructing the accelerator.

Using the methodology in [4], the nested loops in Listing 1 are transformed into a new set of loops in Listing 2, illustrated as a datapath in Figure 4. The  $I_{buf}$ ,  $O_{buf}$  and  $W_{buf}$  arrays represent on-chip buffers for input, output and weight data, respectively. These buffers function as data caches to reduce off-chip memory access; copying data in or out of these arrays represents transferring data between these buffers and main memory. For simplicity, Listing 2 does not show a required boundary check when copying data. Double-buffering is used to overlap data transfer with computation and requires provisioning each memory with twice the capacity.

The loops  $R$ ,  $C$ ,  $M$  and  $N$  are tiled with factor  $T_r$ ,  $T_c$ ,  $T_m$  and  $T_n$  respectively. These loop tiling factors control how much data is transferred per buffer refill/write-out, and the order in which data is transferred. Since the inner-most two loops are unrolled (based on  $T_m$  and  $T_n$ ), loop tiling also controls how the compute modules are constructed. In particular, to implement these two unrolled loops,  $T_m$  vector dot-product units are constructed, each of width  $T_n$ . An accumulation adder is added after each unit, as shown in Figure 4. This yields  $T_m T_n$  multipliers and adders.

Given a resource budget (e.g., a number of DSP slices), one can find the optimal  $T_n$  and  $T_m$  for a given convolutional layer. In [4], a joint optimization is performed to create a single CLP to compute *all* of the convolutional layers in the CNN. The

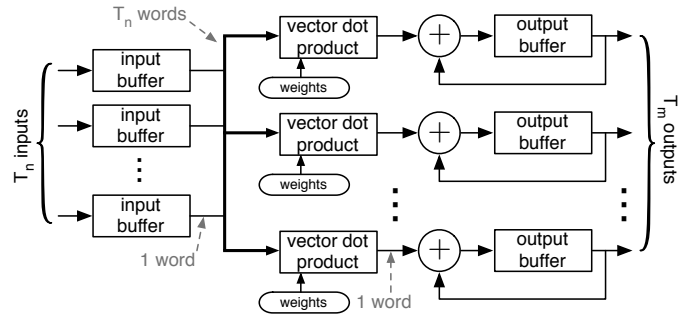


Fig. 4. A convolutional layer processor (CLP), based on the design in [4]. Each dot-product unit takes in  $T_n$  inputs and  $T_n$  weights and produces one output.

optimization finds the  $(T_n, T_m)$  that maximize the aggregate performance of the CLP.

### B. DSP Slice Utilization Problem

Although the methodology in [4] produces a design optimized for the collective performance of all convolutional layers, we observe that its speed is limited by the fact that the different convolutional layers of the CNN have different dimensions, but all are computed on the same  $(T_n, T_m)$  CLP. Thus, the CLP that gives the best performance *across all layers* is not necessarily well suited for any one layer. Because the limiting factor of the system performance is the amount of parallel arithmetic in the CLP, a good way to quantify the cost of this mismatch is to examine the dynamic utilization of the DSP slices used in the floating point arithmetic units. That is, we can quantify the percentage of the time that the DSP slices in the CLP are doing work versus the percentage of the time they are idle. Such analysis shows that the DSP slices of the best design in [4] are active less than 75% of the time, limiting the throughput to under 75% of the maximum that could potentially be reached given the DSP slices used. When we repeat this for the larger Virtex-7 690T FPGA, utilization falls to 65.4%.

The primary cause of the utilization penalty is a mismatch between the tile parameters  $(T_n, T_m)$  and their corresponding loop sizes  $(N, M)$ . In particular, if  $N$  ( $M$ ) is not a multiple of  $T_n$  ( $T_m$ ), then there must be cycles where some of the  $T_n \times T_m$  multipliers are not used. For example, the design in [4] targets the AlexNet CNN [3] and uses 2,240 DSP slices. For this network and resource budget, the optimum  $(T_n, T_m)$  is  $(7, 64)$ . However, the  $(N, M)$  of layers 2a and 2b are  $(48, 128)$ . Because 7 does not evenly divide 48, in  $1/7$ th of the cycles, the arithmetic units are underutilized; during this time,  $6/7$ ths of the DSP slices remain idle. Thus, the overall utilization of this layer on this CLP is  $6/7 + (1/7)(1/7) = 88\%$ .

Even lower utilization is seen when  $T_n > N$  or  $T_m > M$ , resulting in underutilized DSP slices on every cycle. For example, the first layer of AlexNet has  $(N, M) = (3, 48)$ , but because the CLP design is  $(7, 64)$ , the utilization is only  $(3/7)(48/64) = 32\%$ . Overall, analyzing all convolutional layers used in [4] gives a dynamic DSP slice utilization of

74.1%. Moreover, in Section VI we show that this underutilization problem grows with the number of available DSP slices.

#### IV. MULTI-CLP STRUCTURE AND OPTIMIZATION

To improve the dynamic resource utilization and thus CNN performance, we propose Multi-CLP accelerators, where the available resources are partitioned across several smaller convolutional layer-processors rather than a single large one. The advantage comes from the CLPs having different sizes, more closely matching the dimensions of the CNN layers. This approach is possible because CNN accelerators process many input images, allowing CLPs to concurrently work on independent inputs.

To construct a Multi-CLP accelerator for a given resource budget and CNN structure, one must decide how many CLPs to use, how to partition the resources among them, and how to distribute and schedule the processing of individual convolutional layers from multiple images on the CLPs. We describe the operation of a Multi-CLP, a model to predict CLP costs and performance given its parameters, and an optimization algorithm to find the best Multi-CLP design for a given resource budget and set of CNN layers.

##### A. Multi-CLP Accelerators for CNNs

Due to the feed-forward nature of the CNN structure, it is natural to think of the layers of the CNN as a pipeline. Therefore, one way to construct an accelerator with multiple CLPs is to implement one CLP per layer. An accelerator for an  $L$ -stage CNN would have  $L$  CLPs and would operate on  $L$  independent input images. (That is, CLP1 would work on image  $i$  while CLP2 works on image  $i - 1$ , etc.) This would have the benefit of allowing each CLP to be optimized solely for the dimensions of one CNN layer, improving efficiency. In this example, every CLP must still read its inputs from and write its outputs to off-chip memory, because each layer requires different data orderings than the previous layer produces, and the data sizes are typically too large to hold on chip.

A limitation of this approach, however, is that it requires the number of CLPs to be equal to the number of convolutional layers. This poses several problems for practical CNNs. First, it forces the design to divide the on-chip BRAM resources, reducing the buffer size of each CLP. As a result, the ability to exploit data reuse in each CLP diminishes, slowing each CLP and greatly increasing the whole overall memory bandwidth requirement. Second, this one-to-one mapping of CLPs to convolutional layers requires coordinating a large number of accesses to off-chip memory, which is costly in terms of performance and logic resources. Third, each CLP has an overhead cost (e.g., control logic for address calculation and loop index counting). If there are many CLPs, extra resources (especially DSP slices) would be used for control logic instead of CNN computation.

To address these problems, we consider a Multi-CLP design with  $P$  CLPs, where  $1 \leq P \leq L$  (for a CNN with  $L$  layers). Such an approach requires a single CLP to compute multiple CNN layers. We assume the assignment of layers to CLPs

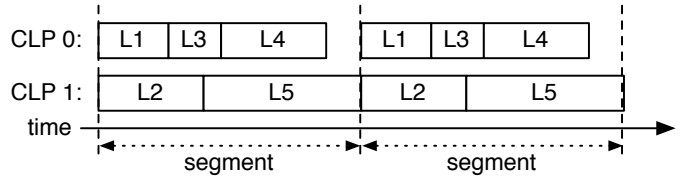


Fig. 5. Example of a Multi-CLP system with two CLPs.

is static, with each layer strictly assigned to a specific CLP. Layers assigned to the same CLP need not be adjacent in the CNN structure.

The timeline of the accelerator operation is divided into *segments*. In each segment, each CLP sequentially processes its layers, with each layer having its own independent data. The segment ends when all CLPs finish. Figure 5 shows an example where CLP0 processes three layers (L1, L3, and L4) and CLP1 processes two (L2 and L5). In each segment, each CLP only consumes data generated during the *previous* segment, avoiding data dependencies within a segment. For example, the output produced by L1 in segment  $i$  will be used as input for L2 in segment  $i + 1$ . This means that processing an image requires 5 segments of time, therefore data from 5 different images will be in-flight at any time.

There are several considerations for a Multi-CLP system to achieve high throughput; we use these as the targets of our optimization method (Section IV-C). First, the segment length, and thus the system throughput, is limited by the CLP that takes the longest to complete its assigned work. For example, in Figure 5, CLP0 is idle after it finishes L4 until the next segment begins. Second, the convolutional layers assigned to a CLP should have dimensions compatible with the CLP dimensions, to ensure high dynamic DSP utilization. Third, the on-chip memory allocated to each CLP is inversely related to the bandwidth it requires; larger CLP buffers reduce off-chip data transfer.

##### B. Modeling CLP Cost and Performance

To find the optimal Multi-CLP design, we first construct a model of the CLP costs (DSPs, BRAMs, memory bandwidth) and speed (cycles), given the CLP parameters and the layers it must compute. A CLP is parameterized by its size ( $T_n, T_m$ ) and the tiling parameters ( $T_r, T_c$ ) of each of its layers (see Table I in Section VI for an example). The model also uses the dimensions of the convolutional layers:  $M, N, R, C, K$  and  $S$  (see Section II). From these parameters, one can derive the resource use and performance of a CLP. Because our CLP is based on [4], variations of many of the formulas used in our models below appear there, but with meaningful differences.

**Performance Model.** Assuming a fixed frequency, the performance of a CLP is dictated by the number of cycles needed to compute each of its layers. Because arithmetic units may be underutilized, the cycle count can not be calculated by dividing the amount of work with the number of arithmetic units. Instead, an exact counting of loop iterations based on Listing 2 is needed. In Listing 2, the innermost two loops

are unrolled, thus they do not contribute to loop iterations. Along the  $R$  dimension, the outer loop (looping over tiles) and inner loop (looping over elements in a tile) combined have  $R$  iterations. Similarly, there are  $C$  iterations along that dimension. The remaining four loops have  $\lceil \frac{M}{T_m} \rceil$ ,  $\lceil \frac{N}{T_n} \rceil$ ,  $K$  and  $K$  iterations, respectively. Together, the cycles needed to compute one layer is

$$Cycles = R \times C \times \lceil \frac{N}{T_n} \rceil \times \lceil \frac{M}{T_m} \rceil \times K^2. \quad (1)$$

**Modeling Bandwidth Usage.** We are primarily interested in the peak bandwidth use of a CLP, to estimate how much bandwidth is needed to avoid computation being blocked by data transfer. If a CLP needs to compute multiple layers, the peak bandwidth use is decided by its most bandwidth-intensive layer. For the computation of a single layer, double-buffering allows complete overlap of computation with data transfer, thus the difference between peak bandwidth and average bandwidth is negligible, and can be computed as the amount of data transferred during the computation of the layer divided by time needed to compute that layer. The amount of data transferred can be calculated by tracking buffer refills and write-outs.

The input buffer and weight buffer are each refilled  $N_{ib} = N_{wb} = \lceil \frac{R}{T_r} \rceil \cdot \lceil \frac{C}{T_c} \rceil \cdot \lceil \frac{M}{T_m} \rceil \cdot \lceil \frac{N}{T_n} \rceil$  times. Each time, the input buffer needs  $D_{ib} = T_n((T_r - 1)S + K)((T_c - 1)S + K)$  words (single-precision floats, in our case), and the weight buffer needs  $D_{wb} = T_n \cdot T_m \cdot K^2$  words. The output buffer is written out  $N_{ob} = \lceil \frac{R}{T_r} \rceil \cdot \lceil \frac{C}{T_c} \rceil \cdot \lceil \frac{M}{T_m} \rceil$  times, and  $D_{ob} = T_m T_r T_c$  words are transferred each time. Each bias is transferred only once, and there are  $M$  of them. The bandwidth use (in words/sec.) for computing a single layer is

$$Bandwidth = \frac{(D_{ib}N_{ib} + D_{wb}N_{wb} + D_{ob}N_{ob} + M)}{Cycles/Frequency}. \quad (2)$$

**Modeling DSP Slice Usage.** Our primary use of DSP slices is the  $T_m$  dot-product units (each of size  $T_n$ ) and  $T_m$  accumulator adders (see Figure 4); each compute module contains  $T_m T_n$  multipliers and adders. Each floating-point multiplier requires 2 DSP slices and each adder requires 3. Therefore, the DSP count is

$$NumDSP = (3 + 2) \times T_n T_m. \quad (3)$$

**Modeling BRAM Usage.** BRAMs are used to construct input, weight, and output buffers. Modeling this must account for the banking of buffers, the number of read/write ports a buffer uses, whether double-buffering is used, and the capacity and capabilities of BRAM. In the following model, we report usage in terms of Virtex-7 BRAM-18Kb units, which can store 512 words (4 bytes each) and operate in ‘‘Simple Dual-Port mode’’ [6], which allows one read and one write concurrently.

The input buffer is organized into  $T_n$  banks of size  $B_i$ , which is provisioned to support the computation of all of the layers on this CLP. When computing a layer, each bank stores  $((T_r - 1)S + K)((T_c - 1)S + K)$  words. Since these

parameters change from layer to layer, each layer can require a different amount of data. So,  $B_i$  is large enough to support the most demanding layer. An input bank must be double-buffered to support the overlapping of computation and data transfer, using one read port and one write port. This buffer bank is constructed with  $2 \cdot \lceil \frac{B_i}{512} \rceil$  BRAMs. However, because a single BRAM already provides a read port and a write port, when  $B_i \leq 256$ , a single BRAM can be used to construct a double-buffered input bank.

The weight buffer is quite similar to the input buffer. There are  $T_n T_m$  banks. When computing a layer, each weight bank stores a  $K \times K$  filter ( $K^2$  words). Thus the largest  $K$  that the CLP needs to handle decides the size of a weight bank. Other aspects of weight banks are identical to that of input banks, thus they are constructed and modeled in the same way.

The output buffer is organized into  $T_m$  banks. When computing a layer, each bank stores  $T_r T_c$  words. Like the other buffer banks, the output buffers are double-buffered and are provisioned for the most demanding layer. However, in order to support the accumulation used in the CLP, an output-buffer bank requires two BRAMs for double-buffering. Therefore, even when the size of an output-buffer bank is less than 256 words, two BRAM-18Kb units are needed to build it. Other than this, the construction and model of the output buffer banks is the same as that of input and weights.

Bias values are not stored in BRAM because the total number of biases is small and many are accessed in parallel.

**Potential Model Improvements.** Our model is based only on an analytic understanding of the CLP and how its resources are mapped to an FPGA. There are several ways the model can be improved. First, we are modeling only the DSP slices used in the CLP compute modules. However, additional DSPs are consumed by addressing and control logic. Second, when we estimate the cycle count of each CLP, we do not take into account the cycles required each time the pipeline needs to be refilled. Third, we are not distinguishing between memories implemented as block RAMs (typical) or distributed RAMs (rarely). In Section VI, we measure the accuracy of our model and show that the omission of these details only causes small differences between the model predictions and the implementation. Additionally, we are not modeling the FPGA flip-flops or LUTs; in our experiments, we were never limited by the number of available flip-flops or LUTs.

### C. Optimization of Multi-CLP Designs

We now describe an optimization tool that uses this model to find the fastest Multi-CLP configuration (for a given CNN) that fits in a set of resource constraints. Since we are specifically targeting FPGAs, we optimize our accelerator only for one specific target CNN. However, in principle this optimization could be applied over multiple target CNNs, jointly optimizing their performance.

This optimization takes as inputs the CNN layers to be accelerated and a set of resource constraints and produces a Multi-CLP configuration. This specifies all parameters of the accelerator: the number of CLPs and the parameters of

---

```

procedure OptimizeMultiCLP(cnn,  $N_{dsp}$ ,  $N_{bram}$ , bw)
  step = 0.01
  target = 1.00
  while (1)
     $Cycle_{target} = \frac{Cycles_{min}}{target}$ 
     $A = OptimizeCompute(cnn, N_{dsp}, Cycle_{target})$ 
    if ( $A = \emptyset$ )
      target = (target - step)
      continue
    else
       $A' = OptimizeMemory(cnn, N_{bram}, bw, A)$ 
      if ( $A' = \emptyset$ )
        target = (target - step)
        continue
      else
        return PickBest( $A'$ )

```

---

Listing 3. Multi-CLP CNN Accelerator Optimization Procedure.

each ( $T_n$  and  $T_m$ ). It also outputs the distribution of the CNN layers to the CLPs, and for each layer, the ( $T_r, T_c$ ) parameters, which dictate how the layer is computed by the CLP (see Section III-A).

Given a set of parameters, evaluating the model is extremely simple. However, there are far too many possibilities to do an exhaustive search for the fastest design that meets the resource requirements. Instead, we have constructed an algorithm that uses dynamic programming and an iterative refinement of the performance goal. The system first calculates a lower-bound on the number of cycles  $Cycles_{min}$  for the entire Multi-CLP by computing the overall number of arithmetic operations required for the CNN ( $2 \cdot \sum_i N_i M_i R_i C_i K_i^2$  summed over all convolutional layers), and divides it by the number of arithmetic operations that can fit in the given DSP budget. This system then aims to find configurations that can finish as close to this lower bound as possible without violating resource constraints.

Listing 3 shows this procedure, which we have implemented as a C++ program. The *OptimizeCompute* function aims to find all solutions that fit within  $N_{dsp}$  DSPs and finish in up to  $Cycle_{target}$  cycles. For each potential solution it finds, it returns: the number of CLPs, the ( $T_n, T_m$ ) of each, and the assignment of layers in *cnn* to the CLPs. Then *OptimizeMemory* takes candidates produced by *OptimizeCompute* and finds all possible solutions that will fit within the given BRAM and bandwidth budgets. This step determines the  $T_r$  and  $T_c$  parameters used for each layer, which dictate the number of BRAMs and memory bandwidth used. Note that one candidate in  $A$  may result in several solutions in  $A'$ ; this is because a given configuration from *OptimizeCompute* may have several sets of ( $T_r, T_c$ ) that fit within the budgets. If no valid solutions can be found after either of these two steps, the procedure increases  $Cycle_{target}$  (lowers the throughput goal) and repeats the process. The granularity by which  $C_{target}$  is increased after each failed iteration is user-specified; in the code shown here, we reduce the DSP slice utilization target (and thus throughput) by 1% each step.

We apply dynamic programming to both

*OptimizeCompute* and *OptimizeMemory* functions, which greatly reduces optimization runtime. For example, optimizing a Multi-CLP accelerator for AlexNet on the Virtex-7 690T takes less than one minute. As a final step, *PickBest* chooses the best solutions from  $A'$ . This works by first eliminating sub-optimal designs (e.g. if two designs have different numbers of BRAMs, but the exact same throughput and bandwidth, we will drop the one with extra unhelpful BRAMs). Then, the “best” point can be found, where best can be defined in several ways (e.g. the highest overall throughput or the lowest BRAM usage while being within 1% of the fastest design observed). Lastly, we note that we can also adapt this method to optimize Single-CLP systems by simply constraining *OptimizeCompute* to only consider solutions with one CLP.

## V. DESIGN AND IMPLEMENTATION

The optimization algorithm (Section IV) determines the characteristics for an optimized Multi-CLP accelerator, producing a set of constants used to parameterize a C++ high-level-synthesis (HLS) template. The template is compiled to synthesizable Verilog using Vivado HLS 2015.4.2. Our optimizer works on any set of CNN layers and resource budget, and our template supports computation over arbitrary data types. This section describes the CLP template and the steps to ensure the intended hardware is correctly inferred by the HLS tool.

### A. Convolutional Layer Processor Template

The accelerator template is constructed based on nine parameters:  $T_n$  and  $T_m$  to size the CLP compute module,  $M_{max}$ ,  $K_{max}$ ,  $in_{size}$ , and  $out_{size}$  to size the on-chip bias, weight, input, and output buffers, and  $NP$ ,  $WP$ , and  $MP$ , computed from the bandwidth requirements to specify the number of AXI4 ports for transferring input, weight, and output data.

Each CLP produced with the HLS tool has an automatically-generated AXI4-Lite slave interface to trigger the start of computation and multiple AXI4 master interfaces for reading and writing data. For the Multi-CLP designs, each parameterized CLP template is passed through the HLS tool separately, producing independent IP cores that can then be inserted into the top-level system and interconnected using a standard AXI crossbar.

The top level of the CLP template supports up to twelve AXI4 master ports. One port is used only at the start of CLP operation to perform a burst transfer of a 32-byte descriptor containing the arguments for the computation ( $R, C, M, N, K, S, T_r, T_c$ ). After these arguments are retrieved and the derived arguments are computed (e.g.,  $r_{steps}, c_{steps}, m_{steps}, n_{steps}$ ), the design executes the four nested loops shown in Listing 4.

Each iteration of the top-level loops performs computation for a single input tile. The *DATAFLOW* directive indicates that the operations inside the  $n$  loop should be pipelined using ping-pong buffers for concurrently accessed data structures. The *in* feature maps and *weights* are read on every iteration

---

```

compute():
#pragma ARRAY_PARTITION out(1),in(1),bias(1),weights(1,2)
  for (ij = 0; ij < K × K; ij++)
    for (tr = 0; tr < rloops; tr++)
      for (tc = 0; tc < cloops; tc++)
#pragma PIPELINE
      for (tm = 0; tm < Tm; tm++)
        for (tn = 0; tn < Tn; tn++) out[tm][tr][tc] =
          ((ij = 0 && n = 0)?bias[tm] : out[tm][tr][tc]) +
          weights[tn][tm][i][j] × in[tn][S × tr + i][S × tc + j]
write_output():
  for (wr = 0; wr + 1 = n_steps && wr < [Tm/MP]; wr++)
    for (p = 0; p < MP; p++)
#pragma UNROLL, LOOP_MERGE
    xfer(out[[Tm/MP] × p + wr])
TOP():
  transfer_arguments_descriptor()
  for (r = 0; r < r_steps; r++)
    for (c = 0; c < c_steps; c++)
      for (m = 0; m < m_steps; m++)
        for (n = 0; n < n_steps; n++)
#pragma DATAFLOW
        read_bias() // omitted for brevity
        read_input() // omitted for brevity
        read_weights() // omitted for brevity
        compute()
        write_output()

```

---

Listing 4. Accelerator template pseudo-code.

using the ping-pong buffers to allow transferring the subsequent iteration’s data while computation is in progress. The *out* feature maps use ping-pong buffers to allow the start of the subsequent computation while the transfer of the previous output is in progress; however, the  $n + 1 = n_{steps}$  condition prevents transfer on all but the last input tile. Bias transfer is similarly limited to occur only on the initial iterations to avoid unnecessary transfers.

All transfer functions perform the maximum-length contiguous bursts allowed by the data structures to minimize port idle time for initiating transfers. To minimize the number of bursts performed, we prioritize the  $n$  dimension over the  $m$  dimension of the *weights* array, as the CLP designs have  $T_n$  smaller than  $T_m$ . The *read\_input()*, *read\_weights()*, and *write\_output()* functions are parameterized to support concurrent transfers across multiple ports by partitioning the transfers according to the top array dimension as demonstrated in *write\_output()*.

The *PIPELINE* directive in *compute()* unrolls the  $T_m$  and  $T_n$  loops to create the CLP compute module. To ensure concurrent access to the data, the *out*, *in*, *bias*, and *weights* arrays are partitioned across different memory banks. The  $K \times K$  loops are the outer-most dimension to avoid back-to-back (“loop-carry”) data dependencies across loop iterations. *rloops* and *cloops* equal  $T_r$  and  $T_c$ , except the last iteration of the  $r$  and  $c$  loops, in which case *rloops* and *cloops* take the boundary into account.

## B. HLS Quirks

Vivado HLS was instrumental to implement the CNN accelerators presented in this work. However, we faced a number of HLS tool challenges with the CLP design. We encountered

several cases of HLS tool bugs and excessively conservative decisions that would result in broken or sub-optimal designs. Overcoming these problems typically required rearranging and massaging the code to avoid errant behavior. However, in a number of cases, we found no way to instruct the tool to produce the desired design. In the interest of supporting reproducibility of our work, we document the key intricacies of the HLS implementation and the post-processing steps we perform on the resulting Verilog to yield properly working CLPs.

Although the dimensions ( $T_n, T_m$ ) of the compute module are static, the way they are used changes when processing different layers on the same CLP. In particular, the number of tile loop iterations  $r_{steps}, c_{steps}, m_{steps}, n_{steps}$  are determined by the arguments passed in the descriptor on each accelerator invocation. The HLS tool properly pipelines the design if these values are known during synthesis. However, if the values are variables, the tool behaves conservatively and fails to properly pipeline the design, introducing unnecessary task ordering and stalls. To overcome this problem, we use easily-identifiable constants in the HLS template and then perform a post-processing step on the Verilog code to substitute the known constants with names of the registers that hold the argument values. This change results in a correctly operating and properly pipelined design that supports a dynamically-specified number of tile loop iterations.

A dual-ported ping-pong buffer for the *out* feature map array is sufficient to simultaneously perform read and write operations from the *compute()* module and read operations from the *write\_output()* module. This would be achieved by placing the *write\_output()* function outside of the  $n$  loop, rather than suppressing its output on all but the last iteration inside the  $n$  loop. However, we found no combination of HLS directives that could produce a design without conservatively inferring false dependencies and inserting unnecessary stalls. Instead, we placed the *write\_output()* operation inside the  $n$  loop and post-processed the resulting Verilog code to alter the behavior of the generated *out* ping-pong buffer module. We augmented the ping-pong buffer with a counter to make it appear as a deep FIFO to the rest of the design, while internally implementing the ping-pong buffer functionality needed for the correct operation of the CLP design.

We found a problem with how Vivado performs BRAM inference on memories with non-power-of-two depth. This problem (documented by Xilinx [7]) extends a memory’s depth up to the next power-of-two size, potentially adding useless BRAMs to the system. For example, in one experiment, we required nine 32-bit wide memories of depth 8,466. These memories should consume 17 BRAMs each. However, the tools rounds this up to 32, wasting 15 BRAMs in each of 9 memory modules. We scripted the fix suggested in Xilinx [7]; it splits up non-power-of-two memory structures into a collection of smaller memories. For example, the 8,466-deep memory is replaced with one 8,192-depth memory (16 BRAMs) and one 274-depth memory (1 BRAM).

Finally, we note that using the *DATAFLOW* directive with

AXI4 interface ports forces designs that specialize ports to either be read-only or write-only. Because AXI4 ports support completely independent concurrent operations, it is possible to reduce the number of interface ports from the CLP to the AXI4 crossbar by merging the corresponding signals from pairs of read-only and write-only ports.

## VI. EVALUATION

We evaluate the Multi-CLP approach to CNN accelerator design by conducting a case study of implementing AlexNet [3] on two Xilinx Virtex-7 FPGAs (485T and 690T). We use our optimization method (Section IV) to determine the best Single-CLP and Multi-CLP designs for each chip’s available resources, implement the designs using the HLS-based method (Section V), and use simulation, synthesis, and place and route tools to compare the two methods and evaluate our models.

Our results demonstrate that the Single-CLP design found by our optimization is equivalent to the optimized result from [4], and that the Multi-CLP methodology yields accelerators with 1.3x and 1.5x higher throughput than the Single-CLP approach (on the 485T and 690T respectively), with a commensurate increase in either block RAM consumption *or* memory bandwidth. Additionally, we find that our model predictions for resource usage and performance closely match the implemented results. We finish our evaluation in Section VI-E by using our model and optimization framework to evaluate how the Single-CLP and Multi-CLP design methodologies scale as future FPGAs grow in computational capacity. We conclude that a Multi-CLP design can give up to a 3.3x improvement in throughput over a Single-CLP design when FPGAs scale up to 9,600 DSPs.

### A. Methodology

We use the optimization procedure (Section IV-C) to find the highest-throughput Single-CLP and Multi-CLP designs for AlexNet on each target FPGA. This process took less than 30 seconds on one CPU. AlexNet (shown in Figure 2) has ten convolutional layers, organized into five matched pairs which we refer to as 1a, 1b, 2a, 2b, etc. We target a clock rate of 100MHz, which we assume in our throughput and bandwidth results.

As input to the optimization procedure, we set the DSP and BRAM budgets to be 80% of the target’s capacity: on the 485T, 1,648 BRAMs (18Kb) and 2,240 DSPs; on the 690T, 2,352 BRAMs and 2,880 DSPs. The 20% headroom is needed because the optimization procedure only considers DSPs and BRAMs used by the compute module and buffers. Additional resource (e.g. DSPs used for address calculation) are not included in the model. Furthermore, routing can become quite challenging as the FPGA resources become fully utilized; with the provided headroom, all designs considered here fulfill the required timing constraints. Additionally, we constrain the memory bandwidth to 4.5GB/s, the maximum practical bandwidth available in [4]. (In practice, our results stay far below this constraint.)

### B. Single-CLP vs Multi-CLP Optimization Results

Next we compare the costs and performance of the Single-CLP and Multi-CLP systems for the two FPGA platforms. Table I presents the parameters chosen by the tool for each system. In each table,  $T_n$  and  $T_m$  give the parallelism of the compute module (Figure 4) and  $T_r$  and  $T_c$  control the on-chip data tiling (Section III-A).

Because we use the design in [4] as the baseline for our CLPs, our Single-CLP system on the 485T has the same parameters,  $T_n = 7$  and  $T_m = 64$ , and the same speed, 2.0 million cycles.<sup>2,3</sup> Accenting the fairness of the comparison, we note that the Single-CLP and Multi-CLP designs have the same arithmetic cost, which the Multi-CLP design spreads among several CLPs. Recall that a CLP requires  $T_n \times T_m$  multipliers and adders. For example, on the 690T FPGA, the Single-CLP design uses  $9 \times 64 = 576$  multipliers and adders in one CLP. The corresponding Multi-CLP design uses the same number ( $1 \times 48 + 3 \times 48 + 1 \times 128 + 4 \times 64 = 576$ ), but distributes them over four different CLPs.

The tables also show which of the 10 convolutional layers of the network, shown in Figure 2, map to which CLPs. Interestingly, although the resources of the 485T and 690T FPGAs are not drastically different, the optimization tool finds very different Multi-CLP solutions for these two platforms. On the 485T, it uses three CLPs, mapping layers 1a and 1b to CLP0, layers 2a and 2b to CLP1, and the remaining six layers to CLP2. On the 690T, the optimizer finds a less-regular solution. Here, the best Multi-CLP solution decomposes the layers differently, splitting up the paired layers to different CLPs (e.g., layer 2a is computed on CLP2 while layer 2b is computed on CLP3).

To understand why this happens, it is useful to consider the cycle counts for each CLP. The last column of each table shows the number of cycles (in terms of cycles $\times$ 1000) that each CLP takes to execute its layers, with the overall cycles per image for each system at the bottom. For the Single-CLP designs, the overall cycle count is simply the sum of how long the CLP takes to compute each of the ten layers. When two layers are listed together (such as 4a and 4b), the cycle count is the number of cycles needed to execute each of those layers. For example, CLP3 in the 690T Multi-CLP design executes four layers: 2b, 3a, 3b, and 5b. The overall time for this CLP is  $437 + 292 + 292 + 146 = 1,166$  thousand cycles.

In the Multi-CLP system, the CLPs operate concurrently. The cycles for the overall accelerator is the maximum of its individual CLPs, because it dictates the segment length (the interval in which the pipelined Multi-CLP system is able to start a new image). For example, in the 690T Multi-CLP design, the four CLPs have cycle counts of 1098,  $366 + 389 + 389 = 1144$ ,  $875 + 292 = 1167$ , and  $437 + 292 + 292 + 146 = 1167$  thousand cycles, giving an overall time of 1167 thousand cycles.

<sup>2</sup>The cycle counts in [4] only account for half of the convolutional layers (i.e., layers 1a, 2a, ..., 5a of Figure 2 but not layers 1b, 2b, ..., 5b). We therefore double the cycle count in Table 4 of [4] to compare with our implementation.

<sup>3</sup>We cannot verify  $T_r$  and  $T_c$  with prior work [4] as they are not reported.



TABLE I  
OPTIMIZED SINGLE-CLP AND MULTI-CLP ACCELERATORS.

	$T_n$	$T_m$	Layers	$T_r$	$T_c$	Cycles( $\times 1000$ )
CLP0	7	64	1a, 1b	14	19	366
			2a, 2b	14	27	255
			3a, 3b	13	13	169
			4a, 4b	13	13	128
			5a, 5b	13	13	85
Overall						2,006

(a) 485T Single-CLP

	$T_n$	$T_m$	Layers	$T_r$	$T_c$	Cycles( $\times 1000$ )
CLP0	3	24	1a, 1b	28	28	732
CLP1	8	19	2a, 2b	27	27	765
CLP2	7	32	3a, 3b	13	13	338
			4a, 4b	13	13	256
			5a, 5b	13	13	170
Overall						1,531

(c) 485T Multi-CLP

	$T_n$	$T_m$	Layers	$T_r$	$T_c$	Cycles( $\times 1000$ )
CLP0	9	64	1a, 1b	11	19	366
			2a, 2b	14	27	219
			3a, 3b	13	13	132
			4a, 4b	13	13	100
			5a, 5b	13	13	67
Overall						1,769

(b) 690T Single-CLP

	$T_n$	$T_m$	Layers	$T_r$	$T_c$	Cycles( $\times 1000$ )
CLP0	1	48	1a	14	28	1,098
CLP1	3	48	1b	11	28	366
			4a, 4b	13	13	389
CLP2	1	128	2a	9	27	875
			5a	13	13	292
CLP3	4	64	2b	9	27	437
			3a, 3b	13	13	292
			5b	13	13	146
Overall						1,167

(d) 690T Multi-CLP

Because our optimization system maximizes the overall throughput, the Multi-CLP designs it produces tend to be balanced, like this example. This balance indicates that the resources are effectively spread across the computation pipeline, such that each CLP can be kept busy most of the time. Table II shows the dynamic DSP utilization of each design, as well as the modeled consumption of DSPs, BRAMs, and bandwidth. We see that, on both FPGAs, the Multi-CLP systems provide a significant throughput advantage over the Single-CLP: 1.31x on the 485T and 1.51x on the 690T. Because the Single- and Multi-CLP designs use an equal number of DSPs, the speedup is proportional to the Multi-CLP improvement in dynamic DSP utilization. The 485T and 690T Single-CLP designs are only able to provide useful work to the DSP slices 74.1% and 65.4% of the time, respectively, while the Multi-CLP designs bring these values up to 97.1% and 99.0%. The Gflop/s rate (in the last column) is proportional to throughput.

As the throughput rises, so does the on-chip memory required. On the 485T FPGA, the 1.31x throughput improvement comes at a cost of 1.22x higher BRAM usage. On the 690T, the throughput improvement of the Multi-CLP designs grows to 1.51x, requiring 1.46x higher BRAM usage. It's natural that, as the rate of computation increases, the amount of data that must be kept on-chip will also increase commensurately. However, it is interesting to note that there is actually a tradeoff between the number of BRAMs used and off-chip memory bandwidth required. We can save bandwidth by adding more input and output buffers, or we can reduce the size of those buffers at the cost of higher bandwidth.

We illustrate this phenomenon in Figure 6, showing the op-

TABLE II  
MODEL-PREDICTED RESOURCE USE AND THROUGHPUT OF SINGLE-CLP AND MULTI-CLP ACCELERATORS ON XILINX VIRTEX-7 485T AND 690T. BANDWIDTH AND THROUGHPUT ASSUME A 100MHZ CLOCK.

	BRAM	DSP	B/w (GB/s)	DSP Util. (%)	Thr. img/s	Gflop/s
<b>485T</b>						
Single-CLP	730	2,240	1.47	74.1	49.85	66.3
Multi-CLP	891	2,240	1.49	97.1	65.32	86.9
<b>690T</b>						
Single-CLP	866	2,880	1.89	65.4	56.54	75.2
Multi-CLP	1,264	2,880	1.88	99.0	85.65	113.9

tions for the two Multi-CLP systems. The Multi-CLP designs shown in Table II were chosen to match the memory bandwidth used by the Single-CLP system. However, one could also adjust this tradeoff, saving BRAMs while using more bandwidth. All alternatives for each system have near identical throughput (e.g., all 690T designs share the 85.65 image/sec throughput shown in the table, with differences bounded by *step* in Listing 3), but each gives different BRAM/bandwidth choices. For example, the points labeled A and C correspond to the iso-bandwidth designs described above. Another useful example is represented by the points labeled B and D, which allow the Multi-CLP designs to match the BRAM utilization of the Single-CLP systems, at the expense of bandwidth. Point B reduces the 485T Multi-CLP BRAM usage to 729, but increases the bandwidth requirement to 1.61 GB/s. On the 690T FPGA, Point D represents an alternate design using only 866 BRAMs, but requiring a bandwidth of 3.44 GB/s. Given specific bandwidth and BRAM constraints, the optimization

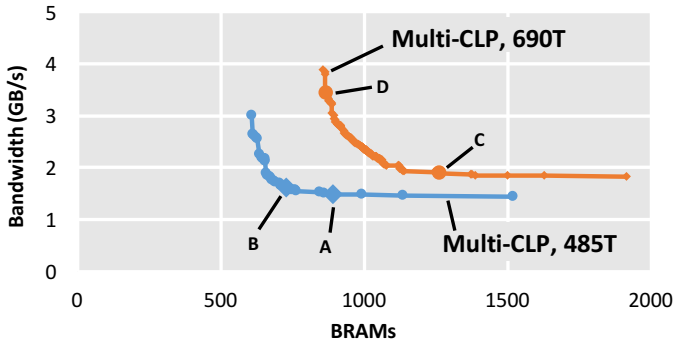


Fig. 6. Illustration of the tradeoff between BRAM usage and off-chip memory bandwidth required for Multi-CLP designs.

TABLE III  
COMPARISON OF MODEL PREDICTION AND IMPLEMENTATION RESULTS FOR SINGLE-CLP AND MULTI-CLP SYSTEMS ON 485T AND 690T.

	BRAM		DSP		Cycles( $\times 1000$ )	
	model	impl.	model	impl.	model	impl.
<b>485T Single-CLP</b>						
CLP0	730	730	2,240	2,331	2,006	2,036
<b>485T Multi-CLP</b>						
CLP0	336	336	360	438	1,464	1,465
CLP1	260	260	760	832	1,531	1,536
CLP2	295	71	1,120	1,199	1,527	1,579
Overall	891	667	2,240	2,469	1,531	1,579
<b>690T Single-CLP</b>						
CLP0	866	866	2,880	2,981	1,769	1,794
<b>690T Multi-CLP</b>						
CLP0	174	174	240	314	1,098	1,099
CLP1	312	312	720	803	1,145	1,160
CLP2	386	386	640	705	1,167	1,174
CLP3	392	392	1,280	1,350	1,167	1,186
Overall	1,264	1,264	2,880	3,172	1,167	1,186

tool or the designer can choose between different points along the tradeoff line.

### C. Model Predictions vs Synthesized Hardware

We synthesized and implemented (place and route) the HLS-based designs described in Section V. The designs target a 100 MHz clock, meeting all timing constraints. Table III compares our model predictions with the implementation results in terms of BRAMs, DSPs, and cycles. For the Multi-CLP systems, we present the metrics of each CLP in addition to the overall values for the entire Multi-CLP design. Note that the “overall” cycle count for the Multi-CLP systems is the maximum time of its CLPs, while the overall DSPs and BRAMs are the sum.

The model predictions are extremely close to the implemented system. Divergence from the implementation results is minor, at most 3% in terms of cycles and at most 9% in terms of DSP counts. The difference in cycle counts arises entirely from the overheads of pipeline refills at the beginning of each input tile. The difference in the number of DSP slices is also expected; the model underestimates by approximately 70–80 DSP slices per CLP, as our model accounts only for the

TABLE IV  
FPGA RESOURCE UTILIZATION FOR THE SINGLE-CLP (S-CLP) AND MULTI-CLP (M-CLP) SYSTEMS OPTIMIZED FOR 485T AND 690T.

	485T		690T	
	S-CLP	M-CLP	S-CLP	M-CLP
BRAM-18K	730 (35%)	667 (32%)	866 (29%)	1,264 (43%)
DSP	2,331 (83%)	2,469 (88%)	2,981 (83%)	3,172 (88%)
FF	154,813 (25%)	182,964 (30%)	190,782 (22%)	216,444 (25%)
LUT	163,896 (54%)	182,394 (60%)	206,566 (48%)	260,499 (60%)

DSP slices used in the compute module for the convolution arithmetic, and does not include DSP slices that used in address calculations and loop indexing. We have also verified that the number of DSP slices used in the compute modules perfectly matches the model prediction.

The BRAM utilization model exactly matches the implementation except in CLP2 of the 485T Multi-CLP system. The difference is due to an assumption in the model that all input, output, and weight buffers are implemented with BRAMs. However in this instance, the number of weights stored in each memory is small, 224 weight memories of only 18 words each. The Vivado tools (sensibly) implement these memories as distributed RAMs (using LUTs and flip-flops instead of BRAMs), causing the model to overestimate BRAM usage by 224 memories.

We conclude that the differences observed between the model and implementation results are not symptoms of the model misunderstanding the design and its requirements. The differences occur because the model does not take into account some toolflow-specific considerations. Several small modifications would allow the model to correct these minor modeling errors, at the cost of making the model toolflow-specific.

### D. CNN Accelerator Resource Utilization

Table IV reports the sum of the resources (including FPGA flip-flops and LUTs) used by each of the designs. These values include the CLPs only, not any platform-specific memory controllers, etc. We note that the Multi-CLP implementations use more DSP slices than the Single-CLP implementations, even though their compute modules (i.e., the arithmetic used for the convolution’s multiplications and additions) use the same number of DSPs. This is because each CLP includes logic for address calculation and loop indexing, adding about 6% more DSP slices to the Multi-CLPs systems. Other increases are seen in the flip-flops and LUT counts; adding more CLPs requires additional logic beyond the DSPs and BRAMs. However, the DSP utilization limits the implementations significantly more than the flip-flops or LUTs.

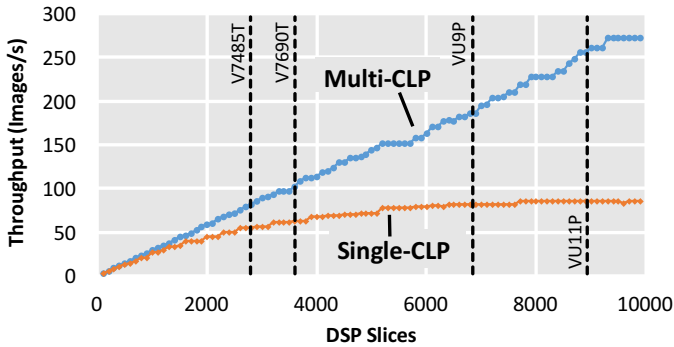


Fig. 7. Throughput for AlexNet CNN on Multi-CLP and Single-CLP designs versus the number of available DSP slices.

### E. Projections to Future FPGAs

In addition to comparing the Single-CLP and Multi-CLP designs targeting Virtex-7 FPGAs, it is also instructive to examine how the Single-CLP and Multi-CLP designs scale as the resource budget grows. For example, the Xilinx roadmap includes UltraScale+ devices with over 10,000 DSP slices. To demonstrate the effect of this trend, Figure 7 shows the throughput of the Multi-CLP and Single-CLP designs for DSP budgets ranging from 100 to 10,000, in steps of 100. For each point, we perform our optimization to find the best Multi-CLP and Single-CLP designs (targeting the convolutional layers of AlexNet) and report the throughput predicted by our model.

The x-axis shows the number of DSP slices for each design. The BRAM budget is set at a ratio of 1 BRAM (18Kb) to every 1.3 DSP slices, an approximation of the relationship we observe in Virtex-7 parts. We constrain all designs in this experiment to use an off-chip bandwidth of at most 4.5GB/sec. Dashed vertical lines illustrate the total number of DSP slices available on two current and two upcoming Xilinx FPGAs: (from left to right) Virtex-7 485T, Virtex-7 690T, Virtex UltraScale+ 9P, and Virtex UltraScale+ 11P. Note that the dashed lines are provided for perspective of resource capacity; real designs, such as our previous case study, would constrain the resources available to the CNN accelerator below the chip capacity.

As the number of available DSP slices increases, the throughput difference between the Single- and Multi-CLP methods grows. For example, at 9,600 DSP slices, the Multi-CLP design has 3.3x higher throughput than a Single-CLP design with identical resource budget. Moreover, if fixed-point arithmetic replaces floating point (as suggested by some recent studies [8]), this greatly increases the number of multipliers and adders available even in existing FPGAs, leading to a similar effect.<sup>4</sup>

Intuitively, our Multi-CLP methodology is most beneficial when the CNN convolutional layers have heterogeneity in the layer dimensions, while homogeneity in the layers mitigates the severity of the dynamic resource underutilization

<sup>4</sup>DSP slices are not necessarily the limiting resource in fixed-point designs. Such designs should be optimized with a cost model modified to account for the resource usage of the fixed-point implementation.

for Single-CLP designs. For example, VGGNet-E [5] has 16 convolutional layers, but there is significant repetition and regularity in the  $(N, M)$  values (e.g., three stages of  $(256, 256)$ , seven stages of  $(512, 512)$ , etc.). For this network, the performance improvement of the Multi-CLP design over a Single-CLP is modest. A 10,000 DSP slice budget improves performance by 1.18x compared to a Single-CLP design.

## VII. RELATED WORK

The baseline Single-CLP design we use in this work is based on [4]. Other recent works have proposed different related types of CNN acceleration hardware. For example, [9]–[12] focus on 2D-convolvers, which play the roles of both compute modules and data caches. Meanwhile, [13], [14] use FMA units for computation. These approaches also differ in the order of data transfer and the choice of memory organization. Despite this, there are a number of important similarities that cause these methods to suffer from the same type of underutilization problem we observe in the Single-CLP. For example, the 2D-convolvers used in [9]–[12] must be as large as the largest filter in any of the CNN layers; they will necessarily be underutilized when used to compute any layer that has smaller filters. As another example, in [13], the organization of the compute modules depends on the number of output feature maps and their number of rows. Because both of these parameters can change drastically from layer to layer, an analogous resource underutilization problem occurs. In these cases, a resource partitioning technique like ours can be employed to improve resource utilization.

We note that several recent works explored other aspects of CNN accelerators. A bandwidth optimization orthogonal to our approach is shown in [15]. This work includes CNN optimization through data quantization (using fewer bits in order to reduce costs) and through a matrix-decomposition method that aims to compress some of the CNN weights. These types of optimizations could be integrated with our approach, since we focus on the organization of computation units themselves. Another recent work [16] explored using an OpenCL-based HLS tool to implement CNN accelerators including the CNN’s pooling and fully connected layers, using smaller fixed-point values. Due to these differences we cannot directly compare our values with [16], although we note that they compute all of their convolutional layers with a single CLP. Lastly, there have been several works related to ASIC CNN accelerators [17]–[22]. Although we focused our evaluation of the Multi-CLP architecture on FPGAs, our technique could be applied to ASIC-based acceleration.

## VIII. CONCLUSIONS

The traditional approach to FPGA-based CNN accelerator design uses a “one size fits all” approach, where a single convolutional layer processor (CLP) is used to compute all convolutional layers of the CNN. In this paper, we observed that variation in the dimensions of the CNN layers limits the throughput of the Single-CLP approach; on layers whose dimensions are a poor fit for the CLP parameters,

the arithmetic units exhibit low dynamic utilization, where adders and multipliers are frequently unused. To overcome this inefficiency, we presented a new design paradigm that partitions hardware resources among multiple cooperating CLPs. Our approach allows the CLP dimensions to more closely match the CNN layer dimensions, resulting in better dynamic resource utilization and higher throughput.

The optimization algorithm we developed finds the optimum Multi-CLP design within a given resource budget (DSP slices, BRAM, bandwidth). On the Virtex-7 485T FPGA, we showed that a Multi-CLP accelerator yields a 1.31x higher throughput compared to the state-of-the-art Single-CLP design. On the Virtex-7 690T FPGA, the improvement increased to 1.51x. The arithmetic units in the Multi-CLP designs have 97% and 99% dynamic utilization, respectively. Further, we showed that the disparity between the throughput of the Single-CLP and Multi-CLP designs grows rapidly as the resource budget increases. For a future FPGA with 10,000 DSP slices and ~7,700 BRAMs, conservatively assuming 4.5GB/s memory bandwidth, our optimization produces a Multi-CLP design with 3.3x higher throughput compared to a Single-CLP using the same resources.

#### ACKNOWLEDGMENT

This material is based on work supported by the National Science Foundation under Grant Nos. 1533739 and 1453460.

#### REFERENCES

- [1] A. Van den Oord, S. Dieleman, and B. Schrauwen, "Deep content-based music recommendation," in *Advances in Neural Information Processing Systems*, 2013, pp. 2643–2651.
- [2] R. Collobert and J. Weston, "A unified architecture for natural language processing: Deep neural networks with multitask learning," in *Proceedings of the 25th international conference on Machine learning*. ACM, 2008, pp. 160–167.
- [3] A. Krizhevsky, I. Sutskever, and G. E. Hinton, "ImageNet classification with deep convolutional neural networks," in *Advances in Neural Information Processing Systems*, 2012, pp. 1097–1105.
- [4] C. Zhang, P. Li, G. Sun, Y. Guan, B. Xiao, and J. Cong, "Optimizing FPGA-based accelerator design for deep convolutional neural networks," in *Proc. FPGA*, 2015, pp. 161–170.
- [5] K. Simonyan and A. Zisserman, "Very deep convolutional networks for large-scale image recognition," *CoRR*, vol. abs/1409.1556, 2014.
- [6] Xilinx, "7 series FPGAs memory resources user guide."
- [7] —, "Vivado synthesis - sub-optimal inference of block RAM (bad area QoR) when the depth is non-power of 2," <http://www.xilinx.com/support/answers/61995.html>, accessed 2016-03-26.
- [8] S. Anwar, K. Hwang, and W. Sung, "Fixed point optimization of deep convolutional neural networks for object recognition," in *ICASSP*, 2015, pp. 1131–1135.
- [9] C. Farabet, C. Poulet, J. Y. Han, and Y. LeCun, "CNP: An FPGA-based processor for convolutional networks," in *Field Programmable Logic and Applications*, 2009, pp. 32–37.
- [10] C. Farabet, B. Martini, P. Akselrod, S. Talay, Y. LeCun, and E. Culurciello, "Hardware accelerated convolutional neural networks for synthetic vision systems," in *ISCAS*, 2010, pp. 257–260.
- [11] M. Sankaradas, V. Jakkula, S. Cadambi, S. Chakradhar, I. Durdanovic, E. Cosatto, and H. P. Graf, "A massively parallel coprocessor for convolutional neural networks," in *Application-specific Systems, Architectures and Processors*, 2009, pp. 53–60.
- [12] S. Chakradhar, M. Sankaradas, V. Jakkula, and S. Cadambi, "A dynamically configurable coprocessor for convolutional neural networks," in *ACM SIGARCH Computer Architecture News*, vol. 38, no. 3, 2010, pp. 247–257.
- [13] M. Peemen, A. Setio, B. Mesman, and H. Corporaal, "Memory-centric accelerator design for convolutional neural networks," in *Computer Design (ICCD)*, 2013, pp. 13–19.
- [14] M. Peemen, B. Mesman, and H. Corporaal, "Inter-tile reuse optimization applied to bandwidth constrained embedded accelerators," in *Design, Automation & Test in Europe*, 2015, pp. 169–174.
- [15] J. Qiu, J. Wang, S. Yao, K. Guo, B. Li, E. Zhou, J. Yu, T. Tang, N. Xu, S. Song *et al.*, "Going deeper with embedded FPGA platform for convolutional neural network," in *Proceedings of the 2016 ACM/SIGDA International Symposium on Field-Programmable Gate Arrays*, 2016.
- [16] N. Suda, V. Chandra, G. Dasika, A. Mohanty, Y. Ma, S. Vrudhula, J.-s. Seo, and Y. Cao, "Throughput-optimized OpenCL-based FPGA accelerator for large-scale convolutional neural networks," in *Proceedings of the 2016 ACM/SIGDA International Symposium on Field-Programmable Gate Arrays*. ACM, 2016, pp. 16–25.
- [17] T. Chen, Z. Du, N. Sun, J. Wang, C. Wu, Y. Chen, and O. Temam, "DianNao: A small-footprint high-throughput accelerator for ubiquitous machine-learning," in *ACM SIGPLAN Notices*, vol. 49, no. 4, 2014, pp. 269–284.
- [18] Y. Chen, T. Luo, S. Liu, S. Zhang, L. He, J. Wang, L. Li, T. Chen, Z. Xu, N. Sun *et al.*, "DaDianNao: A machine-learning supercomputer," in *MICRO*, 2014, pp. 609–622.
- [19] Z. Du, R. Fasthuber, T. Chen, P. Ienne, L. Li, T. Luo, X. Feng, Y. Chen, and O. Temam, "ShiDianNao: shifting vision processing closer to the sensor," in *ISCA*, 2015, pp. 92–104.
- [20] D. Liu, T. Chen, S. Liu, J. Zhou, S. Zhou, O. Teman, X. Feng, X. Zhou, and Y. Chen, "Pudiannao: A polyvalent machine learning accelerator," in *Proceedings of the Twentieth International Conference on Architectural Support for Programming Languages and Operating Systems*. ACM, 2015, pp. 369–381.
- [21] W. Qadeer, R. Hameed, O. Shacham, P. Venkatesan, C. Kozyrakis, and M. A. Horowitz, "Convolution engine: balancing efficiency & flexibility in specialized computing," in *ACM SIGARCH Computer Architecture News*, vol. 41, no. 3. ACM, 2013, pp. 24–35.
- [22] C. Farabet, B. Martini, B. Corda, P. Akselrod, E. Culurciello, and Y. LeCun, "Neuflow: A runtime reconfigurable dataflow processor for vision," in *Computer Vision and Pattern Recognition Workshops*, 2011, pp. 109–116.